The EMBO Journal (2012) 31, 4466–4480 | © 2012 European Molecular Biology Organization | Some Rights Reserved 0261-4189/12
www.embojournal.org

THE EMBO JOURNAL

EMBO open

Molecular basis for SNX-BAR-mediated assembly of distinct endosomal sorting tubules

Jan RT van Weering[1,5], Richard B Sessions[1], Colin J Traer[1], Daniel P Kloer[2,6], Vikram K Bhatia[3,7], Dimitrios Stamou[3], Sven R Carlsson[4], James H Hurley[2] and Peter J Cullen[1,*]

[1]The Henry Wellcome Integrated Signalling Laboratories, School of Biochemistry, University of Bristol, Bristol, UK, [2]Laboratory of Molecular Biology, National Institute of Diabetes and Digestive and Kidney Diseases, National Institutes of Health, Bethesda, MD, USA, [3]Bio-Nanotechnology and Nanomedicine Laboratory, Department of Chemistry and Nano-Science Center, Lundbeck Foundation Center Biomembranes in Nanomedicine, University of Copenhagen, Copenhagen, Denmark and [4]Department of Medical Biochemistry and Biophysics, Umea University, Umeå, Sweden

Sorting nexins (SNXs) are regulators of endosomal sorting. For the SNX-BAR subgroup, a Bin/Amphiphysin/Rvs (BAR) domain is vital for formation/stabilization of tubular subdomains that mediate cargo recycling. Here, by analysing the *in vitro* membrane remodelling properties of all 12 human SNX-BARs, we report that some, but not all, can elicit the formation of tubules with diameters that resemble sorting tubules observed in cells. We reveal that SNX-BARs display a restricted pattern of BAR domain-mediated dimerization, and by resolving a 2.8 Å structure of a SNX1-BAR domain homodimer, establish that dimerization is achieved in part through neutralization of charged residues in the hydrophobic BAR-dimerization interface. Membrane remodelling also requires functional amphipathic helices, predicted to be present in all SNX-BARs, and the formation of high order SNX-BAR oligomers through selective 'tip–loop' interactions. Overall, the restricted and selective nature of these interactions provide a molecular explanation for how distinct SNX-BAR-decorated tubules are nucleated from the same endosomal vacuole, as observed in living cells. Our data provide insight into the molecular mechanism that generates and organizes the tubular endosomal network.

The EMBO Journal (2012) **31,** 4466–4480. doi:10.1038/emboj.2012.283; Published online 19 October 2012
Subject Categories: membranes & transport; structural biology
Keywords: BAR domain; phosphoinositide; retromer; sorting nexin; VPS35

*Corresponding author. The Henry Wellcome Integrated Signalling Laboratories, School of Biochemistry, University of Bristol, Bristol BS8 1TD, UK. Tel.: +44 117 3312193; Fax: +44 117 3312168; E-mail: pete.cullen@bristol.ac.uk
[5]Present address: Center for Neurogenomics and Cognitive Research, Neuroscience Campus Amsterdam, V University, Amsterdam, The Netherlands
[6]Present address: Syngenta, Bracknell, UK
[7]Present address: Novozymes A/S, 2880 Bagsværd, Denmark

Received: 16 May 2012; accepted: 25 September 2012; published online: 19 October 2012

Introduction

Endosomal sorting is an essential process for maintaining cellular homeostasis with deregulated sorting underlying a variety of pathologies, including neurodegenerative diseases and cancer (Huotari and Helenius, 2011). Endosomal sorting is achieved in the tubular endosomal network (TEN), a complex arrangement of tubular and vesicular structures that surrounds the endosomal vacuole (Wall *et al*, 1980). These tubular/vesicular membrane profiles constitute molecularly distinct sorting platforms for the recycling of proteins back to the plasma membrane or to the *trans*-Golgi network (TGN; Geuze *et al*, 1983). How such a complex tubular–vesicular arrangement is generated and how individual tubules maintain their molecular identities during the processes of protein sorting and membrane trafficking remains, on the whole, unclear. One family of proteins providing new insight into these questions is the SNX-BAR subgroup of sorting nexins (SNXs; Carlton and Cullen, 2005; Seet and Hong, 2006; Cullen, 2008; van Weering *et al*, 2010).

SNXs are a large family of proteins classified by the presence of a phosphoinositide-binding phox homology (PX) domain (Cozier *et al*, 2002; Rutherford *et al*, 2006; Teasdale and Collins, 2012). For the SNX-BAR subgroup, the PX domain resides alongside a carboxy-terminal Bin/Amphiphysin/Rvs (BAR) domain (Carlton *et al*, 2004), which forms a rigid curved structure upon dimerization, that binds to membrane surfaces that display the corresponding level of membrane curvature (Peter *et al*, 2004). In combining these low affinity interactions, SNX-BARs utilize co-incidence detection to selectively associate with phosphoinositide-enriched subdomains of the endocytic network that display a high membrane curvature, including the tubular/vesicular structures of the TEN (Cullen, 2008).

Besides sensing membrane curvature, certain BAR domain-containing proteins can elicit vesicle-to-tubule membrane remodelling (Qualmann *et al*, 2011). Consistent with this, the SNX-BAR protein SNX1 drives the formation of membrane tubules *in vitro* (Carlton *et al*, 2004), and is associated with the generation of a tubular subdomain of the TEN that sorts cargo for endosome-to-TGN recycling (Mari *et al*, 2008). Other SNX-BARs are also associated with the generation of distinct tubular subdomains of the TEN. SNX8 mediates endosome-to-TGN recycling via tubular subdomains that are not labelled with SNX1 (Dyve *et al*, 2009), while SNX4 is associated with a tubular subdomain that mediates recycling back to the cell surface (Traer *et al*, 2007; van Weering *et al*, 2012). SNX18 and SNX33 are also associated with tubular subdomains, although their functional role remains controversial (Haberg *et al*, 2008). Although subtle variations may exist between SNX-BARs in binding to phosphoinositides and the sensing of positive membrane curvature, it is unlikely that their functional and spatial separation on the TEN is explained solely through co-incidence detection.

Here, we have systematically examined all mammalian SNX-BARs for their ability to remodel liposomes into membrane tubules in order to gain mechanistic insight into how SNX-BARs regulate the formation and maintenance of distinct tubular subdomains of the TEN. This has revealed that some, but not all SNX-BARs are able to elicit membrane remodelling *in vitro*, and provided evidence that tubule formation requires three basic interactions: BAR domain-mediated dimerization, membrane association and amphipathic helix (AH) insertion, and the formation of higher ordered assemblies through tip–loop contacts. Importantly, the BAR domain-mediated dimerization and tip–loop contacts occur in a restricted manner, which correlates with the known role for individual SNX-BARs in regulating distinct tubular-based recycling pathways. Together, these data provide mechanistic details of how functionally distinct SNX-BAR-coated endosome tubules can be formed from the same endosome vacuole and, in so doing, reveal new insight into the generation and organization of the TEN.

Results

Membrane remodelling features of individual components of the SNX-BAR-retromer complex

The PX-BAR domain unit of several SNX-BAR proteins has been described to contain intrinsic membrane remodelling capacity as shown by their ability to deform liposomes into membrane tubules *in vitro* (Carlton *et al*, 2004; Pylypenko *et al*, 2007; Haberg *et al*, 2008). To systematically screen all full-length mammalian SNX-BARs for their individual ability to remodel membranes into tubular structures, we applied a membrane remodelling assay using Folch liposomes supplemented with PtdIns(3)P (0.3% of total lipid mass). Liposomes were generated by extrusion to form vesicles that appeared as smooth round structures when negatively stained and examined on the electron microscope (Figure 1A). Liposome geometry (average diameter of 185.0 ± 6.5 nm ($n = 55$)) and lipid composition therefore mimicked the PtdIns(3)P-enriched early endosome. Throughout the following study, care was taken to counteract variability in liposome preparations by only comparing data obtained from experiments performed in parallel, on the same day and using the same liposome batch. Positive and negative controls were included in all assays.

Our initial analysis focussed on the SNX-BAR components of the evolutionary conserved SNX-BAR-retromer. In *S. cerevisiae*, the SNX-BAR-retromer is composed of two SNX-BARs, Vps5 and Vps17 (Seaman *et al*, 1998; Cullen and Korswagen, 2012). In vertebrae, these SNX-BARs have undergone gene duplication, with at least two orthologues of Vps5 (SNX1 and SNX2) and two, possibly three orthologues of Vps17 (SNX5, SNX6 and SNX32) (Wassmer *et al*, 2007; 2009; Koumandou *et al*, 2011). Incubation of liposomes with 10 μM of either full-length SNX1 or SNX2 resulted in the formation of tubular structures (Figure 1A). In parallel assays, neither full-length SNX5, SNX6 nor SNX32 was able to induce membrane remodelling.

The inability of these SNX-BARs to induce tubule formation did not result from a defect in membrane association, as sedimentation assays established that all SNX-BAR-retromer components were able to associate with the liposomes (Supplementary Figure S1A). Moreover, increasing the concentration of SNX5 to 100 μM did not change the outcome of the membrane remodelling assay, indicating that SNX5 is incapable of forming stable tubules even at such high concentrations (Supplementary Figure S1D). Finally, to exclude the possibility that the lack of SNX5 tubules arose from an ability of SNX5 to elicit tubule scission thereby generating small vesicles rather than membrane tubules, we spotted the supernatant of the SNX-BAR/liposome mixture onto EM grids after pelleting the large 185 nm liposomes (Boucrot *et al*, 2012). This revealed that the amount of small vesicles in preparations incubated with SNX1, SNX5 or buffer control were similar (Supplementary Figure S2), consistent with vesicles being produced during liposome preparation. The absence of tubules in SNX5-incubated liposomes cannot therefore be explained by potential scission activity of this protein.

We next took advantage of the evolutionary conserved nature of the SNX-BAR-retromer. As discussed above, gene duplication has resulted in SNX1 and SNX2 constituting functional equivalents of yeast Vps5, while SNX5, SNX6 and SNX32 are equivalents of Vps17 (Wassmer *et al*, 2007; 2009; Koumandou *et al*, 2011). Early eukaryotes like Archaeplastida and Excavata lack a VPS17 homologue, therefore in these organisms the retromer SNX-BAR dimer is most likely formed by homodimers of VPS5 homologues (Koumandou *et al*, 2011). As SNX1 and SNX2 are the mammalian equivalents of VPS5, and both are able to elicit tubule formation *in vitro*, we reasoned that an ancient ability to form functional homodimers might be retained in these proteins. With this in mind, we decided to test *Trypanosoma brucei* VPS5 (TbVPS5; these organisms lacks a VPS17 orthologue), *Saccharomyces cerevisiae* VPS5 (ScVPS5; unfortunately we were unable to isolate recombinant ScVPS17 as the expression plasmid was not tolerated by the BL-21 cells (Matthew Seaman, personal communication)), and *Caenorhabditis elegans* SNX1 (CeSNX1) and SNX6 (CeSNX6). Like their mammalian orthologues, TbVPS5, ScVPS5 and CeSNX1 all remodelled liposomes into tubules while the Vps17 orthologue CeSNX6, like human SNX5, SNX6 and SNX32, was unable to achieve this (Figure 1B). These data are consistent with VPS5 orthologues being functionally distinct from VPS17 orthologues in their ability to remodel liposomes into tubules. This is entirely consistent with the lack of conservation of VPS17 in some eukaryotes, and suggests that the ability of SNX-BAR-retromer to drive and/or stabilize the formation of membrane tubules is an ancient characteristic of this protein complex.

To correlate the tubules generate by SNX1 *in vitro* with those SNX1-decorated endosomal tubules observed *in vivo*, we analysed the localization of SNX1 to tubular endosomal structures in HeLa cells by immuno-EM (Figure 1D and E; Mari *et al*, 2008; van Weering *et al*, 2012). The diameter of the SNX1-decorated tubular/vesicular profiles observed in fixed cells corresponded well to the membrane tubules formed by SNX1 *in vitro* (40.5 ± 12.4 and 40.4 ± 6.6 nm, respectively; Figure 1G), indicating that SNX1 induces and/or stabilizes a similar membrane curvature *in vitro* and *in vivo*. Finally, we also tested whether the other evolutionary conserved component of the SNX-BAR-retromer, the VPS26–VPS29–VPS35 trimeric complex, was capable of inducing tubule formation: previous structural analysis of VPS35 having hinted at its potential to form a curved structure and hence contribute to

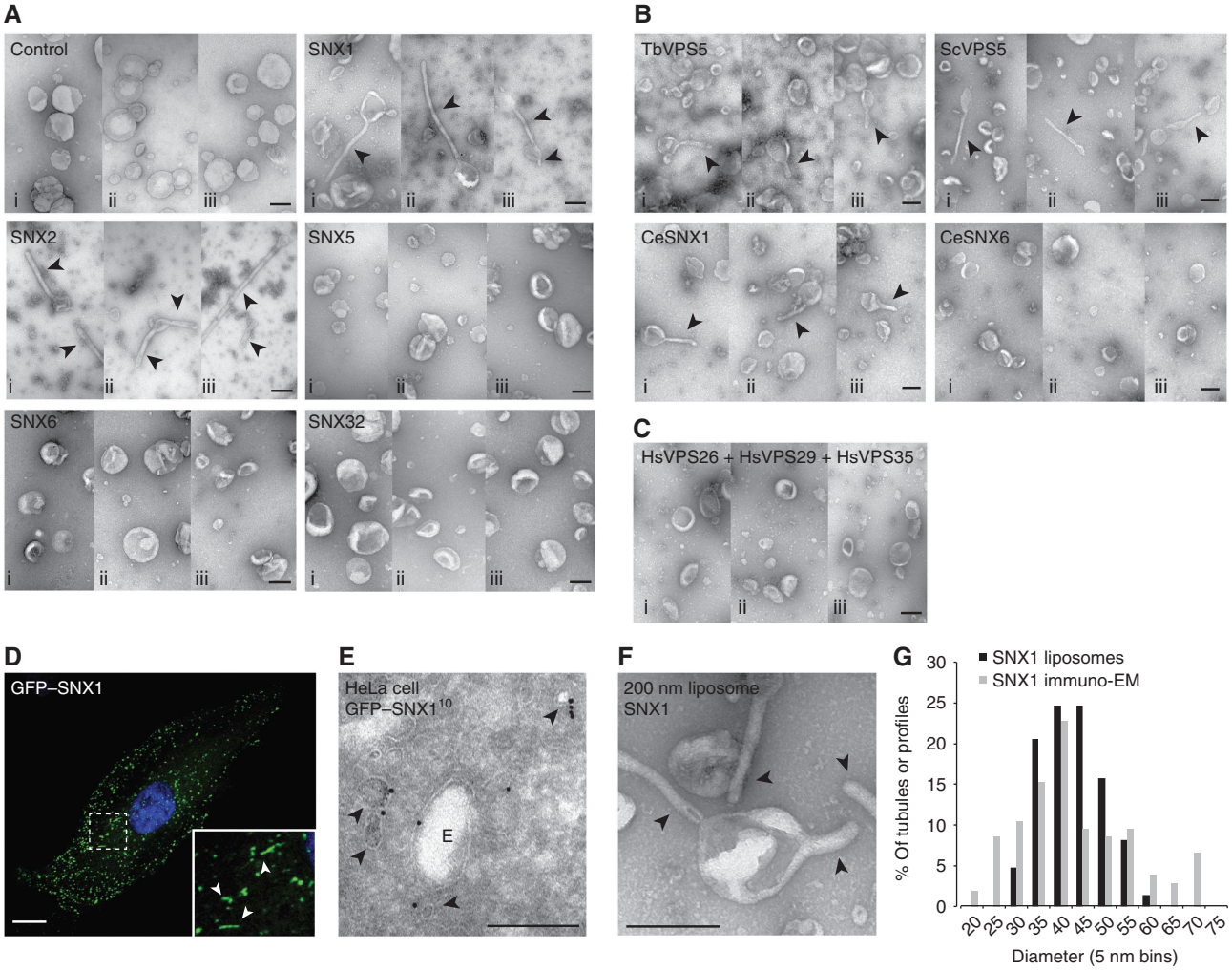

Figure 1 VPS5 homologues of the SNX-BAR-retromer complex remodel liposomes into tubular membrane structures. (**A**) Example micrographs of negative stained liposomes, extruded to 200 nm diameter and incubated with buffer control or the individual SNX-BAR proteins of the mammalian SNX-BAR-retromer complex at 10 μM final concentration (i–iii show three different example views). (**B**) Example micrographs of liposomes incubated with *Trypanosoma brucei* VPS5 (TbVPS5), *Saccharomyces cerevisiae* VPS5 (ScVPS5) or *Caenorhabditis elegans* SNX1 (CeSNX1) and SNX6 (CeSNX6) at 10 μM final concentration (i–iii show three different example views). (**C**) Example micrographs of liposomes incubated with the trimeric complex of *Homo sapiens* VPS26–VPS29–VPS36 (i–iii show three different example views). (**D**) Confocal image of a HeLa cell expressing GFP–SNX1 (green) and stained for nucleus (DAPI, blue). The boxed area indicates the region that is displayed in the insert. Arrowheads indicate GFP–SNX1-positive tubular structures. Scale bar represents 10 μm. (**E**) Electron micrograph of an endosome (marked by 'E') in a HeLa cell expressing GFP–SNX1, which is processed according to the Tokuyasu cryosection method and immunolabelled for GFP-10 nm gold. Arrowheads indicate the tubular/vesicular profiles positive for GFP–SNX1. (**F**) Electron micrograph of liposomes incubated with 10 μM SNX1 at similar magnification as (**E**). (**G**) Histogram of the minimal diameter of SNX1-positive tubular/vesicular profiles in Tokuyasu-processed HeLa cells ($n = 105$) and SNX1-formed tubules on 200 nm liposomes *in vitro* ($n = 49$), plotted as percentage of all tubules in 5 nm bins. All arrowheads indicate the membrane tubules. All scale bars represent 200 nm unless otherwise indicated.

membrane remodelling (Hierro *et al*, 2007; Norwood *et al*, 2010). In our assays, we did not observe any tubules among liposomes incubated with VPS26–VPS29–VPS35, indicating that under these conditions only the evolutionarily conserved VPS5 component(s) of the SNX-BAR-retromer contain intrinsic membrane remodelling capacity *in vitro* (Figure 1C).

Analysis of the remaining SNX-BARs further establishes that not all proteins can elicit vesicle-to-tubule remodelling in vitro

To extend our analysis beyond the SNX-BAR-retromer, we established protocols for the purification of full-length recombinant proteins for each of the remaining seven SNX-BAR family members. SNX9, SNX18 and SNX33 were all able to remodel liposomes into tubular membrane structures (Pylypenko *et al*, 2007; Haberg *et al*, 2008), as were the previously uncharacterized SNX4 and SNX8 (Figure 2A). However, both SNX7 and SNX30 failed to elicit tubule formation in parallel assays, joining SNX5, SNX6 and SNX32 in being unable to induce tubule formation. Again, these SNX-BARs were able to associate with the liposomes, as determined by co-sedimentation, and SNX7 did not induce scission that produces small vesicles rather than tubules (Supplementary Figures S1A and S2). Together, the results indicate that SNX7 and SNX30, like SNX5, lack the intrinsic ability to remodel liposomes into tubules *in vitro*.

Of the SNX-BARs able to elicit tubule formation, SNX1, SNX2 and SNX4 produced tubules of 40–50 nm diameter

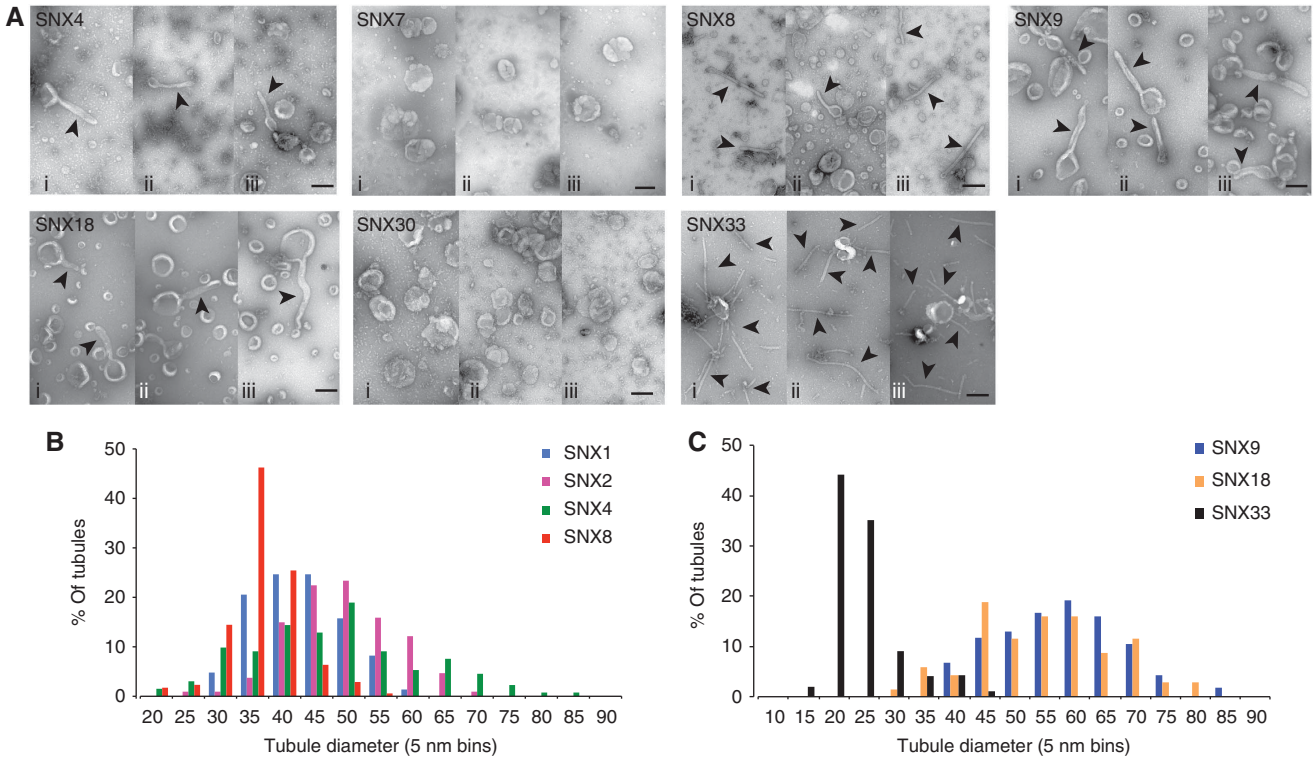

Figure 2 Most SNX-BAR proteins can remodel membranes *in vitro*. (**A**) Example micrographs of negative stained liposomes incubated with the individual SNX-BAR proteins at 10 μM final concentration (i–iii show three different example views), scale bar represents 200 nm. Tubules are indicated by arrowheads. (**B**) Histogram of the diameter of tubules generated by SNX1 ($n = 49$ tubules; see also Figure 1G), SNX2 ($n = 36$), SNX4 ($n = 44$) and SNX8 ($n = 57$), plotted as percentage of all tubules in 5 nm bins. (**C**) Histogram of the diameter of tubule generated by the SH3-SNX-BAR proteins SNX9 ($n = 54$ tubules), SNX18 ($n = 28$) and SNX33 ($n = 114$), plotted as percentage of all tubules in 5 nm bins.

(SNX1 40.4 ± 6.6, $n = 49$ tubules; SNX2 46.9 ± 8.2 nm, $n = 36$; SNX4 44.9 ± 13.1 nm, $n = 44$), while SNX8 produced slightly narrower tubules (33.7 ± 5.3 nm, $n = 57$; Figure 2B). The largest variation in tubule diameter was observed with SNX9, SNX18 and SNX33: both SNX9 and SNX18 produced tubules of large diameter (SNX9 55.2 ± 11.3 nm, $n = 54$; SNX18 52.5 ± 11.3 nm, $n = 23$), while SNX33 produced the thinnest tubules produced by any of the SNX-BARs (21.9 ± 5.7 nm, $n = 114$) (Figure 2C). Whether these distinct tubular profiles are a manifestation of differing BAR domain structures and hence curvature sensing and/or packing of oligomeric assemblies on the tubular surface remains to be clarified. Overall, these data re-enforce that SNX-BARs display a level of functional heterogeneity in their ability to drive membrane remodelling.

SNX-BARs display a restricted pattern of homo- and heterodimer formation

Given that not all SNX-BARs were able to elicit tubule formation, we next examined the ability of these proteins to form homo- versus heterodimers. This stemmed from the observation that the tubulating SNX1 and SNX2 components of the SNX-BAR-retromer are known to form specific heterodimers with non-tubulating SNX5 and SNX6 in order to generate the membrane remodelling unit of the SNX-BAR-retromer (Wassmer *et al*, 2007; 2009). To define the dimerization pattern of the remaining SNX-BARs, we performed a series of co-immunoprecipitation experiments of tagged SNX-BARs expressed in HEK-293T cells. This revealed that SNX4, a protein capable of forming tubules *in vitro*, was able to form homodimers and heterodimers with the non-tubulating SNX-BARs SNX7 and SNX30 (Figure 3A). Confirming this, SNX7 only immunoprecipitated SNX4, while SNX30 primarily immunoprecipitated SNX4 (Figure 3A). No pronounced homodimeric interactions were observed with SNX7 and SNX30, or any of the other SNX-BARs, including those of the SNX-BAR-retromer. SNX4 therefore forms the core component of homodimer SNX4:SNX4, and heterodimeric SNX4:SNX7- and SNX4:SNX30-containing complexes. Indeed, the proposed yeast orthologue of SNX4, Snx4p, is known to form the core of distinct Snx4p:Snx41p and Snx4p:Snx42p sorting complexes (Hettema *et al*, 2003). Based upon sequence comparison and specific dimerization patterns, SNX7 and SNX30 therefore appear to constitute equivalents of yeast Snx41p and Snx42p. The *in vitro* tubulating ability of SNX4 therefore lies at the core of evolutionarily conserved SNX4:SNX7- and SNX4:SNX30-containing complexes, and as such displays function parallels with the respective tubulating versus non-tubulating properties of SNX1/SNX2 and SNX5/SNX6 in the SNX-BAR-retromer.

For the other SNX-BARs, SNX8 predominantly formed SNX8:SNX8 homodimers (Figure 3B), and consistent with evidence that SNX8 regulates endosome-to-Golgi recycling via tubular profiles that are distinct to those labelled with SNX-BAR-retromer (Dyve *et al*, 2009), this SNX-BAR did not form heterodimers with the SNX-BAR-retromer components SNX1 and SNX5 or the SNX4 core component. Finally, turning to the SH3-SNX-BAR family—SNX9, SNX18 and SNX33—conflicting data have been reported on the matter

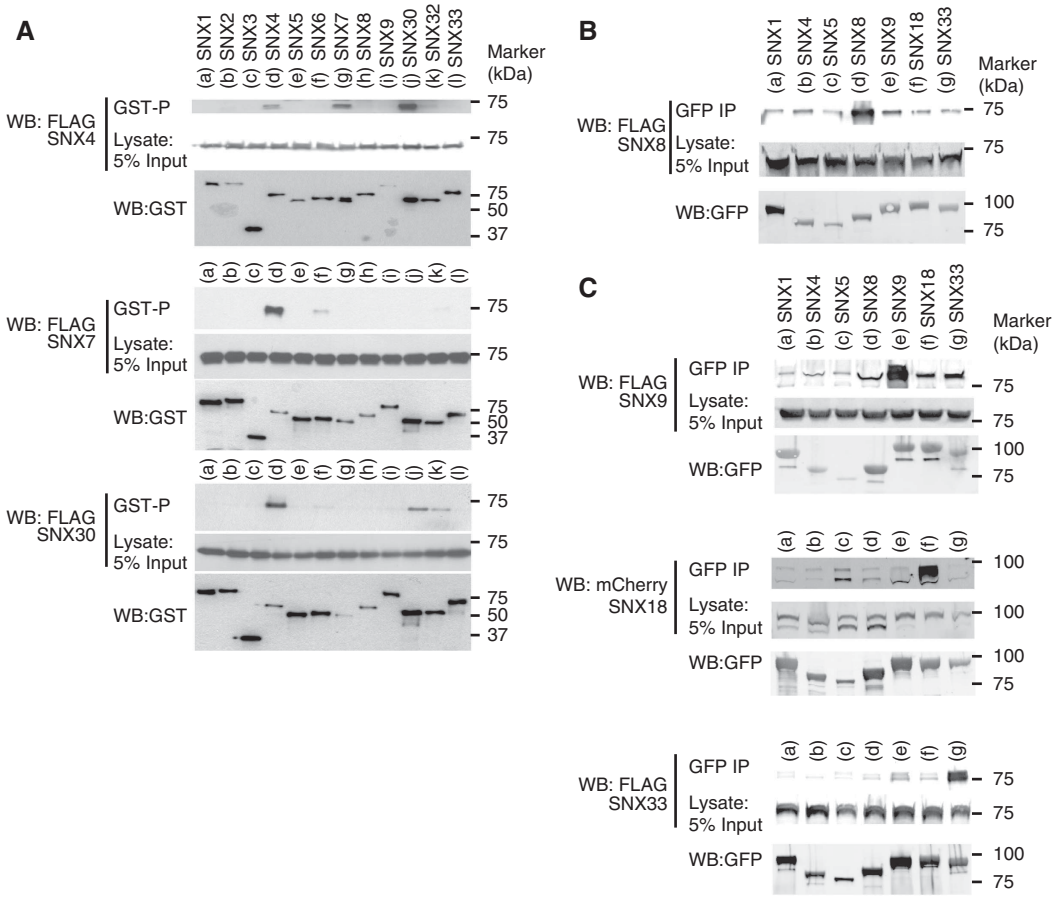

Figure 3 SNX-BAR proteins show a specific pattern of homo- and hetero-dimerization. (**A**) Western blots (WBs) of expressed Flag–SNX4, Flag–SNX7 or Flag–SNX30 co-expressing GST–SNX1 to GST–SNX9, GST–SNX30, GST–SNX32 or GST–SNX33 in HEK-293T cells using glutathione-sepharose precipitation (GST-P). (**B**) WBs of expressed Flag–SNX8 co-expressing GFP–SNX1, GFP–SNX4, GFP–SNX5, GFP–SNX8, GFP–SNX9, GFP–SNX18 or GFP–SNX33 in HEK-293T cells using GFP-nanotrap immunoprecipitation (IP). (**C**) WBs of expressed Flag–SNX9, mCherry–SNX18 or Flag–SNX33 co-expressing GFP–SNX1, GFP–SNX4, GFP–SNX5, GFP–SNX8, GFP–SNX9, GFP–SNX18 or GFP–SNX33 in HEK-293T cells using GFP-nanotrap IP. Figure source data can be found with the Supplementary data.

Table I Data collection statistics

Data set	Native	Hg-edge[a]	Hg-peak[a]
Source	Cu-Kα	BM-22	BM-22
Wavelength (Å)	1.5418	1.00947	0.99187
Unit cell axes (Å)	$a = 89.0$, $b = 118.1$, $c = 61.5$	$a = 89.4$, $b = 119.8$, $c = 61.5$	
Resolution[b] (Å)	40–2.8 (3.0–2.8)	40–3.4 (3.5–3.4)	40–3.6 (3.7–3.6)
Unique reflections	15 254	17 515	14 700
Multiplicity	3.9	4.6	8.6
Completeness (%)	92.0 (91.7)	99.9 (99.4)	99.7 (96.0)
R_{sym} (%)	4.1 (39.3)	10.8 (50.3)	11.7 (40.3)
I/σ_I	23.5 (3.5)	11.6 (2.9)	16.8 (5.8)

[a]Friedel mates treated as separate reflections.
[b]Values in parentheses refer to highest resolution shell.

of homo- versus hetero-dimerization within this SNX-BAR subfamily (Haberg *et al*, 2008; Zhang *et al*, 2009; Dislich *et al*, 2010; Park *et al*, 2010). Under our conditions, we found that SNX9, SNX18 and SNX33 predominantly formed homodimers with minor heterodimerization activity within the SH3-SNX-BAR family (Figure 3C). SNX9 also precipitated SNX8, an interaction that was also observed to a lesser extent in the SNX8 precipitation experiments.

Together, these data establish a restricted series of homo- and hetero-dimerization within the SNX-BAR family. Moreover, when combined with the ability to induce vesicle-to-tubule remodelling *in vitro* (Figure 2A), they reveal a correlation between SNX-BAR homodimer formation and an ability to elicit tubule generation.

Crystal structure of the SNX1 homodimer

To define the molecular details that mediate the specificity of SNX-BAR dimerization and its role in membrane remodelling, we pursued the crystal structures of the SNX1 homodimer and SNX1:SNX5 heterodimer. We were able to determine the structure of the SNX1-BAR homodimer to 2.8 Å (Tables I and II), but were not able to crystallize the SNX1:SNX5

heterodimer. The SNX1-BAR crystals contain one copy of the homodimer per asymmetric unit (Figure 4A). The final model (PDB code 4FZS) contains 209 residues in monomer A (corresponding to residues 305–513 of SNX1; orange in Figure 4) and 191 in monomer B (residues 307–380, 388–435, 443–478, 485–517; cyan in Figure 4). Compared to the SNX9 homodimer (Figure 4B, PDB 2RAK; Pylypenko *et al*, 2007), the SNX1-BAR homodimer has an unusually high degree of curvature that is inconsistent with the diameter of SNX1 membrane tubules, although the correlations are loose rather than strict (Frost *et al*, 2008; Wang *et al*, 2008; 2009). In contrast to SNX9-BAR, which has continuous kinked helices (Figure 4B), SNX1-BAR contains full breaks in helices α2 and α3 (Figure 4A and C). The conventional BAR domain helices α2 and α3 are thus broken up into helices α2/α2′ and α3/α3′ in the SNX1-BAR structure. We speculate that the double breaks in these helices could increase the flexibility of this BAR domain, and may allow it to transiently sample highly curved conformations, which may not be representative of the conformation on membrane tubules. Similar flexibility has been observed in other BAR dimers including the SNX9 PX-BAR domain (Wang *et al*, 2008).

We inspected the SNX1-BAR homodimer interface with a view to understanding why homodimerization is disfavoured relative to heterodimerization *in vivo* (Wassmer *et al*, 2007, 2009). The interface contains a number of charged residues, including His336, Arg337, Glu374 and His381. The closest pair of charged residues to potentially bridge the dimer interface is His336 and Glu374. The His-Glu pair interacts with non-optimal geometry and these residues are 4.5 Å apart, too far for a salt bridge interaction. The positioning of Arg337 is even less optimal. It is in a mostly hydrophobic environment, forming a long hydrogen bond only with a Tyr residue (Figure 4D) and 6.8 Å away from the nearest negatively charged residue, Glu374. The presence of these incompletely neutralized charged residues in a predominantly hydrophobic environment probably explains why the SNX1:SNX1 dimer is disfavoured relative to other interaction modes.

Table II Phasing and refinement statistics

Phasing	
Figure of Merit (SHARP)	
After MAD phasing	0.32
After density modification	0.85
Refinement	
Resolution range (Å)	40–2.8
R_{cryst}/R_{free}[a] (%)	22.8/25.8
Average *B*-factors (Å^2)	85.4
Rms bond lengths (Å)	0.010
Angles (deg)	1.18
Residues in favored/allowed regions[b] (%)	97.9/2.1

[a]R_{free} is calculated for a randomly chosen 5% subset of reflections omitted from refinement.
[b]Assessment of Ramachandran plot using RAMPAGE (Lovell *et al*, 2003).

Non-specific dimerization of SNX-BARs is prevented by charged residues in the hydrophobic BAR-domain interface

As SNX1 is able to elicit tubule formation and has a limited capacity to form homodimers, we decided to investigate the role of charged residues in the specificity of BAR domain-mediated dimerization by examining the non-tubulating, non-homodimerizing SNX5. Although the homology between the SNX1- and SNX5-BAR domain is low (18%) we were able to construct a homology model based on the SNX1 structure (Figure 5A; Supplementary Figure S3). This revealed that two glutamates (Glu280 and Glu383) faced into the otherwise hydrophobic SNX5:SNX5 dimer interface (Figure 5B). To address whether these residues prevent SNX5 homodimerization, we mutated them to alanines (SNX5-AA) and tested their dimerization through immunoprecipitations in HEK-293 cells. In line with earlier reports, we observed strong binding

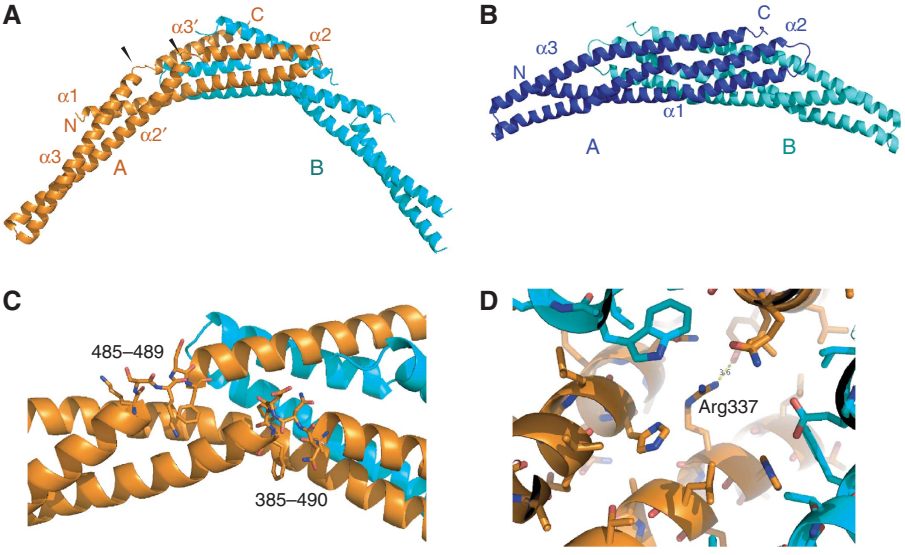

Figure 4 Crystallization of the SNX1 homodimer. (**A**) Ribbon model of the SNX1-BAR homodimer. Chain A is shown in orange and chain B in cyan. Black arrowheads mark the non-standard breaks in BAR domain helices 2 and 3. (**B**) Ribbon model of the SNX9-BAR homodimer (PDB 2RAK; Pylypenko *et al*, 2007) in a similar view as (**A**). SNX9 molecule A is shown in dark blue and SNX9 molecule B in cyan. (**C**) Close-up of the breaks in helices 2 and 3 of the SNX1 structure. (**D**) Close-up of the environment of Arg337 in the SNX1 homodimer, showing that there is no complementary acidic partner residue close enough to neutralize the basic Arg side chain.

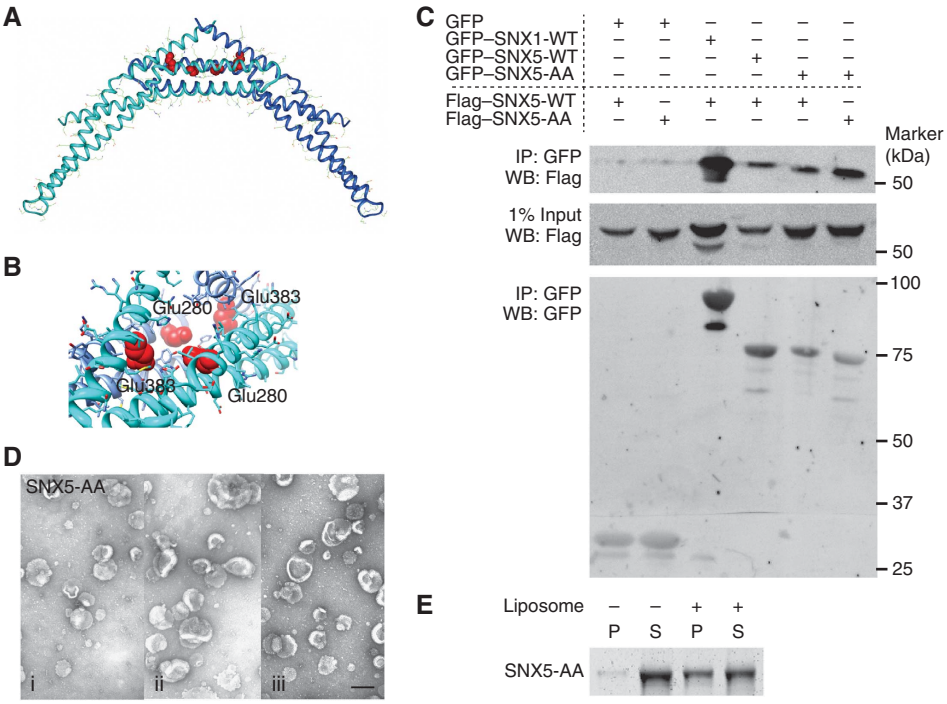

Figure 5 Charged residues in the hydrophobic BAR interface determine specific dimerization of SNX-BAR proteins. (**A**) The homology model of the SNX5:SNX5 homodimer (monomers shown in blue and cyan ribbons). Clashing negatively charged Glu280 and Glu383 are shown as red space filling spheres. (**B**) Close-up of the environment of Glu280 and Glu383 in the SNX5:SNX5 dimerization interface. (**C**) Western blots (WB) of expressed Flag–SNX5 wild type (WT) or Flag–SNX5-E280A/E383A (AA) co-expressing GFP control, GFP–SNX1, GFP–SNX5-WT or GFP–SNX5-AA in HEK-293T cells using GFP-nanotrap IP. (**D**) Example micrographs of liposomes incubated with 10 μM SNX5-AA (i–iii show three different example views), scale bar represents 200 nm. (**E**) Coomassie-stained gel of SNX5-AA in the pellet (P) and supernatant (S) fractions after sedimentation in the presence or absence of liposomes. Figure source data can be found with the Supplementary data.

of SNX5-wild-type (WT) to SNX1-WT, with little affinity for WT SNX5:SNX5 homodimers (Figure 5C; Wassmer *et al*, 2009). In contrast, SNX5-AA precipitated considerably more SNX5-AA than SNX5-WT, although this was not to the same extent as the physiological relevant combination of SNX1:SNX5 (Figure 5C). The Glu280 and Glu383 residues in SNX5 therefore contribute to prevent non-specific SNX5 homodimerization. These results were further validated by the observation that two distantly related SNX-BARs that do not form heterodimers SNX1 and SNX8, form SNX1:SNX8 heterodimers when the charged residues in the BAR-domain interface were changed to hydrophobic amino acids (SNX1-Arg337Leu and SNX8-Gln310Ile; Supplementary Figure S4). Together, these data indicate that charged residues in the BAR-dimerization interface aid to restrict specific dimerization observed in the SNX-BAR protein family.

In generating an SNX5 mutant capable of forming SNX5-AA:SNX5-AA homodimers, we noted that this mutant was unable to remodel liposomes into tubules even though the ability to associate with the liposomes was unaffected (Figure 5D and E). This indicates that simply forming a BAR dimer is not by itself sufficient to remodel membranes *in vitro*. Additional interactions are required.

Membrane remodelling requires the insertion of an AH

SNX-BAR proteins require both the PX domain and the BAR domain to associate with membranes (Carlton *et al*, 2004; Pylypenko *et al*, 2007; Traer *et al*, 2007). In some SNX-BARs, an additional AH has been identified that is important for membrane remodelling and curvature sensing (Pylypenko *et al*, 2007; Bhatia *et al*, 2009). No AHs have been reported in SNX5 or any of the other non-tubulating SNX-BARs, which could explain their inability to remodel membranes. We scanned all mammalian SNX-BAR sequences for putative AHs using HeliQuest (Gautier *et al*, 2008) and identified potential AHs in the N-terminus of the BAR domain in all proteins (Figure 6A; Supplementary Figure S5A). We tested the functional importance of these AHs in the liposome remodelling assay by introducing charged residues in the hydrophobic face of the predicted AHs in SNX1, SNX5 and SNX8 (SNX1 M287E/F288E, SNX5 F186E/F187E and SNX8 V193D/F197D, referred to as 'dAH' mutation; Figure 6B, arrowheads). These mutations did not affect the heterodimerization of SNX1 and SNX5, or the homodimerization of SNX8 (Supplementary Figure S5B and C). SNX1-dAH at 10 μM final concentration failed to remodel liposomes into tubules, while in parallel assays the same concentration of SNX1-WT produced extensive tubules (Figure 6C). When SNX1-dAH was co-incubated with SNX5-WT (5 μM each), the membrane remodelling capacity of the SNX-BAR dimer was restored. Since SNX5-WT alone was unable to induce tubule formation (Figures 1A and 6C), these data suggest that the single AH of SNX5-WT in the SNX1-dAH:SNX5-WT heterodimer is sufficient for membrane remodelling. This was confirmed by the co-incubation of SNX1-dAH with SNX5-dAH, which failed to remodel liposomes into tubules (Figure 6C). All SNX-BAR-dAH mutants were able to associate with liposomes, although to lesser extents as their WT counterparts, indicating that

A

Protein	Region (AA)	Sequence	Reference
SNX1	281–298	GAGLLKMFNKATDAVSKM	Bhatia *et al* (2009)
SNX2	278–295	GAGILRMVNKAADAVNKM	Bhatia *et al* (2009)
SNX4	194–211	TGFQLKADSRLKALNATF	Bhatia *et al* (2009)
SNX5	183–200	FGGFFKSVVKSADEVLFT	This study
SNX6	194–211	EKLEDFFKNMVKSADGVI	This study
SNX7	246–263	GLLSRMGQTVRAVASSMR	This study
SNX8	180–197	SDVQNKLKESAQCVGDEF	This study
SNX9	201–214	MKIPLNKFPGFAKP	Pylypenko *et al* (2007)
SNX18	225–238	VSRNLNRFSTFVKS	Pylypenko *et al* (2007)
SNX30	216–233	IALLTRMGESVKHVTGGY	This study
SNX32	176–192	ELLGGFLRNIVKSADEAL	This study
SNX33	179–192	VGRNLNRFSCFVRS	Pylypenko *et al* (2007)

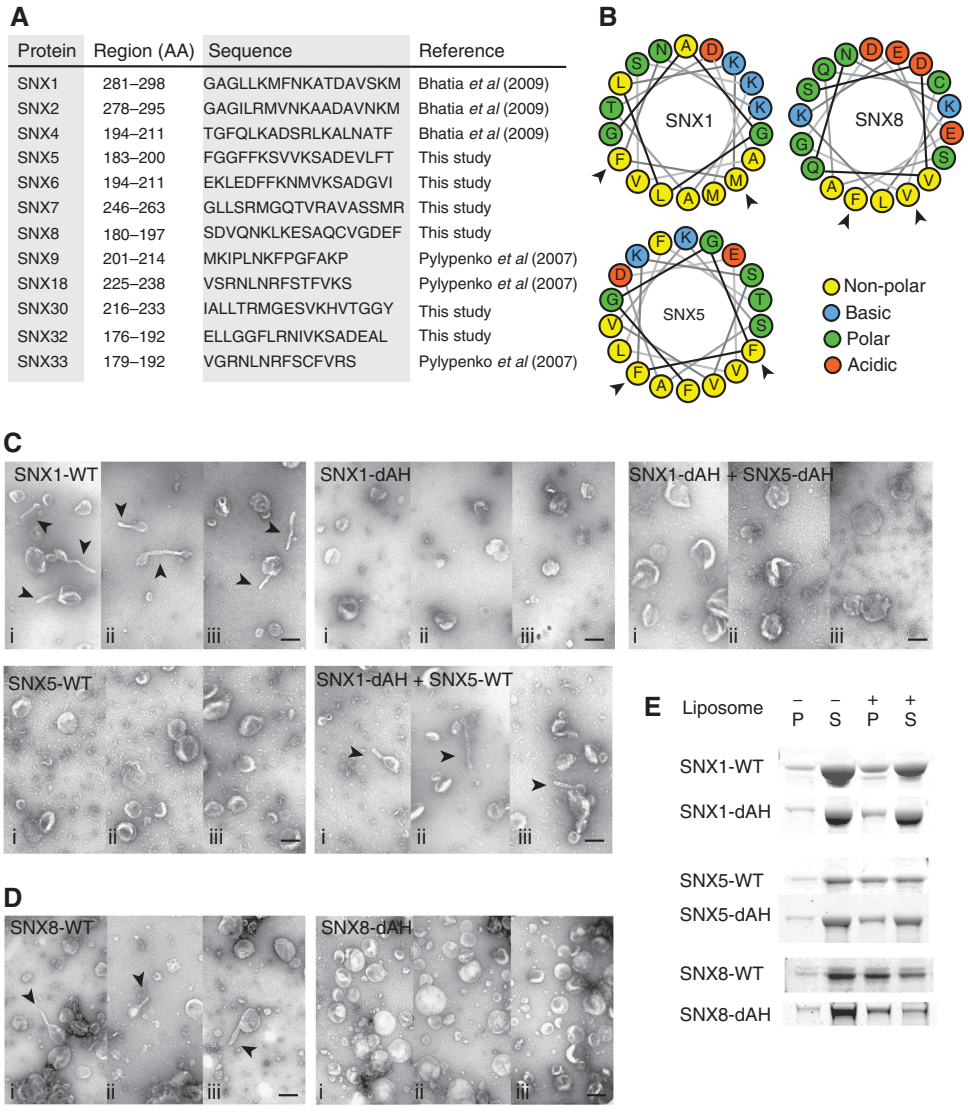

Figure 6 All SNX-BAR proteins contain an amphipathic helix, which is essential for membrane remodelling. (**A**) Table of all predicted amphipathic helices (AHs) in SNX-BAR proteins. The numbers in the region column refer to the amino acids in the full-length protein. (**B**) Cartoon of the arrangement of the 18-residue AHs of SNX1, SNX5 and SNX8. Arrowheads indicate the hydrophobic residues mutated to acidic residues (dAH). (**C**) Example micrographs of liposomes incubated with 10 μM SNX1-WT, SNX5-WT, SNX1-dAH, SNX5-dAH or combinations of SNX1-dAH with SNX5-WT or SNX5-dAH at 5 μM final concentration for each protein (i–iii show three different example views), scale bar represents 200 nm. Tubules are indicated by arrowheads. (**D**) Example micrographs of liposomes incubated with 10 μM SNX8-WT or SNX8-dAH (i–iii show three different example views), scale bar represents 200 nm. Tubules are indicated by arrowheads. (**E**) Coomassie-stained gel of SNX1-WT, SNX1-dAH, SNX5-WT, SNX5-dAH, SNX8-WT and SNX8-dAH in the pellet (P) and supernatant (S) fractions after sedimentation in the presence or absence of liposomes. Figure source data can be found with the Supplementary data.

SNX-BARs with a disrupted AH are still able to undergo membrane association (Figure 6E).

SNX8 contains an AH with a small hydrophobic surface (Figure 6B), which did not initially appear from our bioinformatics screen. To test if this region also behaved like an AH, we introduced negative charge in the hydrophobic face of the SNX8 AH. Similarly to the results on SNX1 and SNX5, the SNX8-dAH mutation perturbed SNX8's ability to remodel liposomes into tubules while liposome association was still evident (Figure 6D and E). This region of SNX8 therefore behaved as an AH and was essential for membrane remodelling. Confirming this, GFP–SNX8-WT induced extensive endosome tubulation when expressed in HeLa cells, while GFP–SNX8-dAH did not induce tubulation even though this mutant retained endosome association (Supplementary Figure S6). Expression of GFP–SNX1-WT also resulted in the formation of extensive GFP-labelled tubular structures in intact cells, in contrast to GFP–SNX5-WT which, although associating with punctae, did not induce a tubulation phenotype: data entirely consistent with the *in vitro* properties of these proteins in remodelling liposomes (Carlton *et al*, 2004; Wassmer *et al*, 2007). GFP–SNX1-dAH and GFP–SNX5-dAH also did not induce tubules when expressed in HeLa cells (Supplementary Figure S6). Interestingly, however, interpretation of these data was limited due to an increased cytosolic distribution compared to their WT counterparts, suggesting that for some SNX-BARs the AH also contributes to *in vivo* membrane association.

Overall, these data established that all SNX-BARs contain AHs that are functionally required for the generation of liposome tubules *in vitro* and *in vivo*. Hence, the BAR domains present in most of the SNXs can be functionally reclassified as being N-BAR domains, with SNX9, SNX18 and SNX33 being considered 'N-BAR domain-like' as the AH lies N-terminally to the PX domain (Peter *et al*, 2004; Gallop *et al*, 2006; Pylypenko *et al*, 2007).

The tip–loop regions of BAR domains are required for SNX-BARs to induce tubule formation

In generating an SNX5 mutant capable of forming SNX5-AA:SNX5-AA homodimers, we noted that this mutant was unable to remodel liposomes into tubules even though it contained functional AHs and the ability to associate with the liposomes was unaffected (Figures 5D, E and 6C). This again indicates that simply forming a BAR dimer is not by itself sufficient to remodel membranes *in vitro* and that an additional interaction is necessary to remodel liposomes into tubules: association between SNX-BAR dimers to form an oligomer that expands local curvature and stabilizes membrane tubules. F-BAR proteins are known to form a higher ordered helical array on membrane tubules by lateral contacts and so-called 'tip-to-tip' contacts between F-BAR dimers (Frost *et al*, 2008). A lysine residue in the loop region between α-helices 2 and 3 of the F-BAR domain is essential for these tip-to-tip contacts and membrane remodelling (Frost *et al*, 2008). We identified two lysine residues in a tip–loop region of the SNX1 BAR domain, Lys442 and Lys445 (Figure 7A) but substitution of these residues for alanines did not affect membrane remodelling or membrane binding (Figure 7B and D), suggesting that SNX1 relies on different residues to form such a predicted higher ordered helical array.

To further test the involvement of the tip-to-tip contacts in SNX-BAR-mediated membrane remodelling, we generated a series of domain swaps between SNX1 and SNX5. Here, we exchanged the tip–loop region of SNX5 (Glu320-Glu345) for the corresponding region in SNX1 (Gln421-Gln462) (SNX5-1TIP; Figure 7A, SNX5 in cyan with SNX1 tip in green). These domains, which have similar charge distributions, mainly differ in their geometry with the SNX1 tip–loop region being more extended (Supplementary Figure S7). Like SNX5-WT and SNX5-AA, SNX5-1TIP was unable to remodel liposomes into tubules, consistent with SNX5's low affinity to form homodimers (Figure 7C). When we introduced the Glu280Ala/Glu383Ala mutation in SNX5-1TIP to allow the formation of homodimers (Figure 5B), SNX5-AA-1TIP was now able to remodel liposomes into tubules (Figure 7C). These experiments show that SNX5-WT, that contains functional AHs but is incapable of remodelling liposomes, can be engineered to an SNX-BAR protein that is capable of vesicle-to-tubule remodelling by allowing SNX5:SNX5 homodimerization and tip–loop associations.

Together, our results are consistent with the ability of SNX-BARs to elicit tubule formation being dependent upon: (i) the ability to form restrictive homo- or heterodimers; (ii) the insertion of an AH into the lipid bilayer; and (iii) the formation of selective higher ordered helical arrays through tip–loop contacts within the BAR domain (Figure 7G). Within the SNX-BAR family the specificity of the tip–loop interactions and BAR domain-mediated dimerization therefore provide a simple mechanism to account for the observed formation of distinct SNX-BAR-decorated tubular profiles of the endosomal network *in vivo* (Traer *et al*, 2007). Indeed, in *in vitro* assay where liposomes were incubated with a premixed combination of full-length recombinant SNX9 (forms 55.2 nm tubules) and SNX33 (forms 21.9 nm tubules) (Figure 2C), we observed two clearly distinct populations of tubules with approximate diameters of 20 and 60 nm (Figure 7E and F). In a reconstituted liposome assay, SNX9 and SNX33 are therefore able to form molecularly distinct tubular structures (Figure 7H).

Discussion

In the present study, we describe the first screen that explores the membrane remodelling capacities of a single family of full-length BAR domain-containing proteins, the mammalian SNX-BAR proteins (see overview of the results in Table III). In documenting how some, but not all SNX-BARs can remodel liposomes into membrane tubules we have revealed a previously unrecognized level of functional diversity within this protein family. Our data are consistent with a three-step model for SNX-BAR-mediated vesicle-to-tubule membrane remodelling: specific hydrophobic and charged interactions in the BAR domain dimer interface determine a restricted pattern of homo- and hetero-dimerization thereby generating specific curved BAR domain dimers; the insertion of an AH is necessary to create local membrane curvature that is subsequently stabilized by the BAR domain; specific tip–loop interactions organize BAR domain dimers into a higher ordered oligomer that extends local membrane curvature into global membrane remodelling. In modifying the non-tubulating SNX5 and thereby engineering a mutant capable of tubule formation, we have provided evidence in support of

Figure 7 Tip connections between SNX-BAR dimers regulate SNX-BAR oligomerization. (**A**) Ribbon model of the SNX1:SNX1 homodimer (green) indicating Lys442 and Lys445 in blue space-filling spheres and the SNX5-AA-1TIP:SNX5-AA-1TIP homodimer (cyan) indicating the tip–loop region of SNX1 in green and the E280A/E383A substitutions in orange space-filling spheres. (**B**) Example micrographs of liposomes incubated with 10 μM SNX1-WT, SNX1-K442A, SNX1-K445A and SNX1-K442/445A (i–iii show three different example views). (**C**) Example micrographs of liposomes incubated with 10 μM SNX5-WT, SNX5-AA, SNX5-WT-1TIP or SNX5-AA-1TIP (i–iii show three different example views). (**D**) Coomassie-stained gel of SNX1-K442A, SNX1-K445A, SNX1-K442/445A, SNX5-WT-1TIP and SNX5-AA-1TIP in the pellet (P) and supernatant (S) fractions after sedimentation in the presence or absence of liposomes. (**E**) Example micrographs of liposomes incubated with 10 μM SNX9, SNX33 or preincubated mixture of SNX9 and SNX33 (i–iii show three different example views). (**F**) Histogram of the diameter of tubule generated by the preincubated mixture of SNX9 and SNX33 ($n = 141$ tubules) plotted as percentage of all tubules in 5 nm bins, in comparison to SNX9 ($n = 54$) or SNX33 ($n = 114$) alone (see also Figure 2C). (**G**) Cartoon of the required interactions by SNX-BAR proteins to remodel membrane vesicles into tubules: (I) formation the SNX-BAR dimer, (II) association of the SNX-BAR dimer with the membrane with insertion of an amphipathic helix and (III) oligomerization of SNX-BAR dimers on the membrane to stabilize and expand local membrane curvature. (**H**) Cartoon of an endosomal vacuole (E) with two SNX-BAR-decorated sorting tubules attached. Each of the sorting tubules will extend selectively by recruitment self similar SNX-BAR molecules, due to the specific dimerization and oligomerization through the BAR domain and tip–loop interactions. All scale bars represent 200 nm. Tubules are indicated by arrowheads. Figure source data can be found with the Supplementary data.

this three-step model. Overall, the highly specific and selective nature of the described interactions provide a simple molecular explanation for how distinct SNX-BAR-decorated sorting tubules can be nucleated from the limiting membrane of the same endosomal vacuole, as has been observed in living cells (Traer *et al*, 2007). In so doing, our data provide new molecular insight into the biogenesis and organization of the TEN.

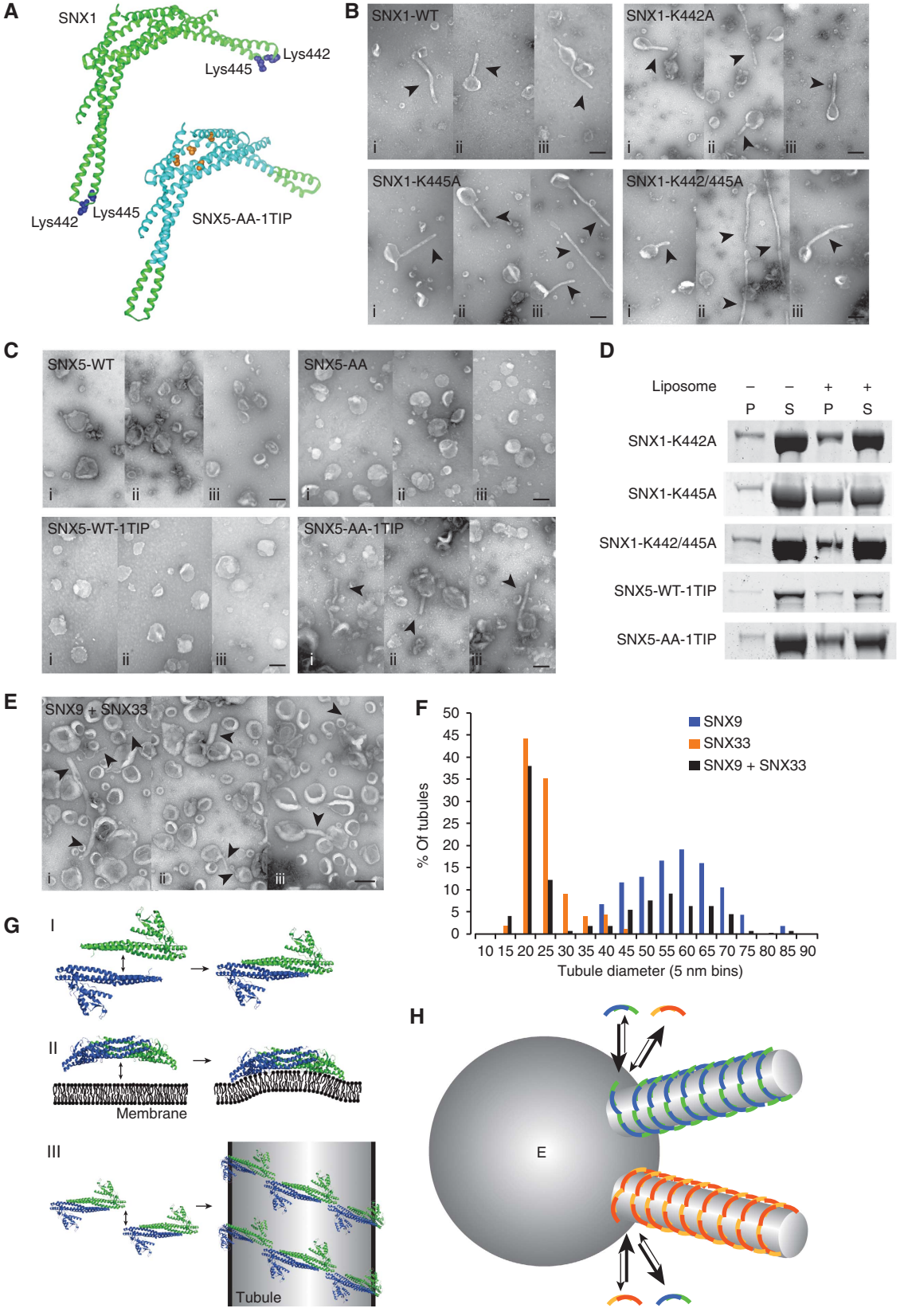

Table III Summary of the membrane remodelling phenotype and dimerization within the SNX-BAR family

	Liposome association	Membrane remodelling	Homodimer	Heterodimer partner(s)
Wild-type protein				
SNX1	+	+	±	SNX5, SNX6 and SNX32
SNX2	+	+	±	SNX5, SNX6 and SNX32
SNX4	+	+	+	SNX7 and SNX30
SNX5	+	−	−	SNX1 and SNX2
SNX6	+	−	−	SNX1 and SNX2
SNX7	+	−	−	SNX4
SNX8	+	+	+	—
SNX9	+	+	+	—
SNX18	+	+	+	—
SNX30	+	−	±	SNX4
SNX32	+	−	−	SNX1 and SNX2
SNX33	+	+	+	—
Mutant protein				
SNX1-dAH	+	−	±	
SNX1-K442A	+	+	Not tested	
SNX1-K445A	+	+	Not tested	
SNX1-K442/445A	+	+	Not tested	
SNX5-AA	+	−	+	
SNX5-dAH	+	−	−	
SNX5-WT-1TIP	+	−	−	
SNX5-AA-1TIP	+	+	+	
SNX8-dAH	+	−	+	

SNX-BARs form a restricted series of homo- and heterodimers that correlates with their ability to elicit tubule formation in vitro

The membrane remodelling phenotype of SNX-BAR proteins corresponds to their dimerization: all those SNX-BARs forming homodimers in cells (SNX8, SNX9, SNX18 and SNX33) and the core subunits of SNX-BAR heterodimers (SNX1, SNX2 and SNX4), that can also form homodimers to some extent, are capable of remodelling liposomes into tubules. All individual SNX-BAR proteins that are found incapable in remodelling membrane *in vitro* (SNX5, SNX6, SNX7, SNX30 and SNX32) nonetheless form heterodimers under physiological conditions with SNX-BAR proteins that contain intrinsic membrane remodelling capacity. We cannot currently exclude that these proteins may contribute to membrane remodelling *in vivo,* although overexpression of SNX5 in HeLa cells clearly does not result in membrane tubulation as is readily observed for SNX1 (Supplementary Figure S6A; Carlton *et al*, 2004; Wassmer *et al*, 2007). For the SNX-BAR-retromer, this is an evolutionary conserved function: the VPS5 homologues of *T. brucei*, *S. cerevisiae*, *C. elegans* and *H. sapien*s are all capable of tubule formation while VPS17 homologues of *C. elegans* and *H. sapiens* are unable to remodel the membrane (Figure 1A and B). This suggests that SNX1 in *C. elegans* and *H. sapiens* has retained some ability to form functional homodimers as is observed for their ancestral VPS5 homologue in *T. brucei* (Koumandou *et al*, 2011). Potentially, the large variety of cargo that requires retromer-based sorting in more complex organisms has driven the need for several retromer-complex variants containing different sets of SNX-BAR heterodimers through which selective retromer cargo traffic can be independently regulated. For example, Shiga toxin is selectively transported by SNX1-containing retromer and is independent of SNX2 (Bujny *et al*, 2007).

The ability to remodel membrane as homodimers is also a property of SNX4 and SNX8. Under physiological conditions, SNX4 preferentially forms heterodimers with SNX7 or SNX30 (Figure 3A). Whether SNX4 or SNX8 has ancient ancestors capable of forming homodimers is unclear as phylogenetic analysis shows that the evolutionary conservation of these SNX-BARs is insufficient for such ancestral genes to be identified (Koumandou *et al*, 2011).

Charged residues in the BAR domain hydrophobic interface help determine the restricted pattern of SNX-BAR dimerization

As a potential molecular mechanism for the restricted pattern of SNX-BAR dimerization, we have identified charged residues in the hydrophobic interface of the newly described SNX1:SNX1 crystal structure and SNX5:SNX5 homology model. Neutralizing these charged residues results in increased homodimerization of SNX5 and heterodimerization of SNX1 with SNX8, suggesting that charged residues play a significant role in restricting dimerization to specific combinations within the SNX-BAR protein family. However, these dimers were not formed to the same extent as the physiological SNX-BAR dimer combination, consistent with other interactions along the extensive hydrophobic interface also contributing to determine the SNX-BAR dimer interaction. Indeed, the formation of SNX9-SNX33 heterodimers requires 19 amino-acid substitutions along the BAR domain dimer interface (Dislich *et al*, 2010) (including similarly positioned charged residues as described in the present study, i.e., Glu457 and Arg559). However, BAR domain dimerization by itself is not sufficient to remodel liposomes into tubules (Figure 5D). Thus, artificially engineered SNX5 homodimers, or the limited formation of SNX30 homodimers (Figure 3A), are both unable to form membrane tubules *in vitro* (Figures 2A and 5D).

The BAR domain of all SNX-BARs contains an AH

Previous reports have shown that SNX9 contains an AH at the N-terminus of its BAR domain, which is important for membrane curvature sensing and membrane remodelling (Pylypenko *et al*, 2007; Bhatia *et al*, 2009). We have observed putative AHs in all SNX-BAR proteins and established for SNX1, SNX5 and SNX8 that these are functionally required for membrane remodelling. All of the SNX-BAR AH mutants tested retained an ability to associate with liposomes, although not as efficiently as the WT protein. When expressed in intact mammalian cells, SNX1-dAH and SNX5-dAH showed an increased cytosolic distribution while SNX8-dAH was present in punctae similar to SNX8-WT. It is unlikely that the difference in membrane association of the dAH mutants *in vivo* is explained by their difference in hetero- and homo-dimerization, since SNX9 AH mutants, that form homodimers and associate with liposomes *in vitro*, also show a predominant cytosolic distribution when expressed in cells (Pylypenko *et al*, 2007). This indicates that the AH contributes to membrane targeting of several SNX-BARs *in vivo*, which is principally governed by the combined phospholipid-binding properties of the BAR and PX domains (Carlton *et al*, 2004). The SNX-BAR proteins should therefore be reclassified as N-BAR-containing proteins (Peter *et al*, 2004; Gallop *et al*, 2006), as such they combine curvature sensing and curvature generation through membrane insertion of amphipathic wedges. The lack of correlation between the hydrophobic moment of the AH

and the observed tubule diameter formed by the different SNX-BAR proteins suggests that the final membrane curvature is mainly determined by the geometry of the SNX-BAR oligomer. Interestingly, in combining SNX1-dAH and SNX5-WT, neither one of which can form tubules on their own, we have obtained evidence that a single functional AH per SNX-BAR-dimer is sufficient to remodel liposomes (Figure 6C).

Tip–loop interactions are necessary for the formation of higher order SNX-BAR assemblies during tubule formation

The presence of a functional AH and dimerization of SNX5 is not sufficient to remodel liposomes into tubules (Figure 5D), suggesting that SNX5 homodimers are unable to form a higher ordered oligomer. F-BAR proteins form such an array through a series of lateral and tip-to-tip contacts (Frost *et al*, 2008). For SNX-BARs, the presence of an SNX-PX domain on the lateral sides of the BAR domain dimer will almost certainly hinder the formation of similar lateral contacts (Pylypenko *et al*, 2007). Therefore, we focused on the properties of the potential SNX1 tip-to-tip contacts. Lys442 and Lys445 in SNX1 are similarly positioned as Lys166 in FBP17, which regulates tip-to-tip contacts in this F-BAR domain-containing protein (Frost *et al*, 2008). These residues are not essential for SNX1-mediated membrane remodelling and similar positioned residues are also present in non-tubulating SNX5 (Supplementary Figure S7), indicating that tip-to-tip contacts of SNX1 are different from those observed in F-BARs. Swapping 40 tip–loop amino acids of SNX1 with the tip–loop of SNX5-AA allowed this chimera to remodel liposomes into tubules, indicating that more extensive tip–loop interactions are required for SNX-BAR-mediated membrane remodelling. Interestingly, the oligomeric lattices of the N-BAR domain of endophilin have recently been shown to be held together not by lateral interactions, but rather by weak tip-to-tip interactions between consecutive N-BAR dimers and promiscuous antiparallel interactions between the AHs of N-BARs in adjacent rows of the lattice (Mim *et al*, 2012). Our data are broadly consistent with such a lattice organization, although the importance of the AHs has not been directly examined in the present study. A detailed cryo-electron microscopy structure of the SNX-BAR lattice formed on the membrane tubule will be required to address the relationship between the tip–loop interactions and the tip-to-tip interaction shown for F-BARs (Frost *et al*, 2008), and also how the PX domain within the PX-BAR unit of SNX-BARs is accommodated by, and contributes to, the lattice organization.

A model to describe for the formation of functionally distinct, SNX-BAR subdomains of the TEN

The work presented here offers insight into the fundamental question of how different SNX-BAR sorting tubules are formed from the same endosome without mixing of their SNX-BAR identity, as is observed for SNX1 and SNX4 in living cells (Traer *et al*, 2007). We propose a model in which the higher order SNX-BAR lattice that drives vesicle-to-tubule remodelling is formed by specific combinations of N-BAR domain-containing SNX-BARs through restricted dimerization in the N-BAR-domain interface and selective tip–loop connections, alongside potential antiparallel interactions between the AHs, that together stabilize the organization of the high order lattice. Hence, while the N-BAR-domain interface determines the formation of SNX8:SNX8 homodimers and SNX1:SNX5 heterodimers, and the combined membrane binding properties of the PX and BAR domains recruited both SNX-BARs dimers to the same membrane, SNX8:SNX8 homodimers will selectively nucleate other SNX8:SNX8 homodimers to form the high order lattice necessary for tubule generation. As SNX8 has little affinity for SNX1:SNX5 heterodimers, this will give rise to an SNX1:SNX5-negative, SNX8-decorated endosomal tubule. In the same way, an SNX8-negative, SNX1:SNX5-decorated endosomal tubule can be nucleated and generated from the same endosomal limiting membrane. By applying these criteria to the remaining SNX-BARs, for example, SNX9 and SNX33 (see Figure 7E and F), one can explain the formation of the observed SNX-BAR-decorated endosomal subdomains. Finally, as individual SNX-BARs directly and/or indirectly associate with various cargo proteins, the formation of such molecularly distinct SNX-BAR coated endosomal tubules will be coordinated with the appropriate selection of cargoes into the correct recycling pathway.

Materials and methods

Plasmids

The different SNX-BAR cDNAs were cloned into pGex6P vector (GE Healthcare, Little Chalfont, UK). The different mutants used in this study were all constructed by PCR-based site-directed mutagenesis and Dpn1 digestion of the parent DNA using the primers listed below.

Removing charged residues in the BAR interface: SNX1R337L forward ttgtagaaactctagtcaaccatctaaaagagctagcgctgaacacagc, reverse gctgtgttcagcgctagctcttttagatggttgactagagtttctacaa; SNX5E280A forward tgaaaaactaaggaaagtagcgggtcgagtttcatcagatg, reverse catctgatgaaactcga cccgctactttccttagtttttca; SNX5E383A forward tctaattgaaatgtctgaactggca ataaaacatgccaggaacaatg, reverse cattgttcctggcatgttttattgccagttcagacattt caattaga; SNX8E310I forward gcacaacagggtaagcaggaaataaacgacgtggtgg agaagc, reverse gcttctccaccacgtcgtttatttcctgcttaccctgttgtgc.

Disruption of the AH: SNX1 (M287E/F288E) forward agtggtgctggt ctcctcaaggaggagaacaaagccacagatgccgtc, reverse gacggcatctgtggctttgt tctcctccttgaggagaccagcaccact; SNX5 (F186E/F187E) forward gagatgt ttggtggcgaggagaaaagtgtggtgaaaagtgctg, reverse cagcacttttcaccacacttt tctcctcgccaccaaacatctc; SNX8 (V193D/F197D) forward gtcagcacagtg cgacggggacgaagacctgaactgtaagc, reverse gcttacagttcaggtcttcgtccccgt cgcactgtgctgac.

Tip-to-tip contacts between SNX-BAR dimers: SNX1K442A forward gctgctgtgggccaacgcgcctgataagctgcag, reverse ctgcagcttatcaggcg cgttggcccacagcagc; SNX1K445A forward ggccaacaagcctgatgcgctgcag caggcca, reverse tggcctgctgcagcgcatcaggcttgttggcc. SNX5-1TIP switches the tip of SNX5 (E320-E345) for that region in SNX1 (Q421–Q462) was made by overlap PCR using primers: SNX5-Nterm forward ccctgggatccatggccgcg, reverse gggcatcctgatagtcaatga gggctttggtgcgtc; SNX5-Cterm forward cgggtgactcaatgctgccagaaatttga acaactttccg, reverse acgatgcggccgctcgagtcg; SNX1-tip forward ccctca ttgactatcaggatgcccaagccacactgc, reverse tctggcagcattgagtcacccgagac tcccactc.

Recombinant protein production

The pGex6P-SNX-BAR constructs were transformed in *Escherichia coli* BL21 cells (Clontech, Mountain View, CA, USA) and grown to 0.8–1.0 OD_{600} cultures. Protein expression was induced by 0.3 μM IPTG at 15°C for 20 h. Cells were lysed in 1% Triton X-100 in PBS by sonication and subsequently pelleted at 16 000 *g*. The protein was harvested by glutathione-sepharose beads (GE Healthcare), the GST tag was subsequently cleaved off by PreScission (GE Healthcare) digestion overnight at 4°C. The protein was further concentrated using centrifugal filters (Millipore Corporation, Billercia, MA, USA). Protein quality and concentration were analysed by Coomassie gel analysis and Bradford assay (Bio-Rad, Hemel Hempstead, UK).

Liposome tubulation and sedimentation assays

Liposomes composed of Folch bovine brain lipids (0.5 mg Sigma B1502, 0.5 mg Avanti Polar Lipids 131101C, supplemented with 3 μg protonated PI(3)P (Avanti Polar lipids LM-1900)) were resuspended at 1 mg/ml by brief sonication in 20 mM HEPES (pH 7.4), 150 mM NaCl, 1 mM DTT at 37°C and sized to ~200 nm diameter by extrusion.

For tubulation assays, 5 μg liposomes were incubated with 10 μM (final concentration) of the protein indicated (10 μl final volume) for 30 min and spotted on a carbon/formvar-coated copper mesh grid. Liposomes were negative stained by 3% uranylacetate for 1 min and analysed on a FEI Tecnai 12 Biotwin transmission electron microscope at × 24 000 magnification. Tubule diameters were quantified in ImageJ analysis software (http://rsbweb.nih.gov/ij/) as an average of three measurements along the tubule.

For sedimentation assays, 15 μg liposomes were incubated with 10 μM (final concentration) of the indicated protein (30 μl final volume) for 30 min and spun down at 170 000 *g* in a Beckman TLA-100 rotor. Supernatant and pellet fractions were collected and analysed by SDS–PAGE visualizing the protein by Coomassie stain.

The formation of small vesicles was tested as described elsewhere (Boucrot *et al*, 2012). Briefly, liposomes were spun down by a 15-min run at 250 000 *g* after a 30-min incubation with the indicated proteins at 10 μM final concentration. The supernatant, containing smaller vesicles, was spotted on a carbon/formvar-coated electron microscopy grid and negative stained by 3% uranylacetate for ultrastructural analysis on a Tecnai 12 Biotwin transmission electron microscope at × 24 000 magnification.

Bioinformatics

Potential AHs were detected using HeliQuest (Gautier *et al*, 2008) at the N-terminal side of the BAR domain as annotated by sequence alignments published elsewhere (Habermann, 2004; Peter *et al*, 2004) or constructed on phylogenetic analysis (Cullen, 2008) in clustalW2 (http://www.ebi.ac.uk/Tools/msa/clustalw2/). The selection criteria was qualitative, allowing linker residues but excluding sequences which were rich in helix breaking residues such as prolines and glycines.

Immunoprecipitation

Combinations of Flag-, GFP- or GST-tagged SNX-BAR protein were expressed in HEK-293T cells for 48 h before lysing the cells in 0.5 ml lysis buffer (0.5% NP-40, 10 mM Tris, 150 mM NaCl, 0.5 EDTA, protease inhibitor; Roche, Burgess Hill, UK). Cell fragments were spun down and the supernatant was incubated with 10 μl washed GFP-trap beads (ChromoTek, Munich, Germany) for 1 h at 4°C. Bound protein was detected by western blotting using Flag (Sigma-Aldrich, Poole, UK), GFP (Roche) or GST (Santa Cruz, Heidelberg, Germany) antibodies.

Light microscopy

HeLa cells were grown in DMEM (Gibco-Invitrogen, Paisley, UK) + 10% fetal calf serum (Sigma-Aldrich) + Penicillin/Streptomycin (PAA, Pasching, Austria) and transfected with the described GFP-fusion constructs using GeneJuice (Millipore Corporation) according to the instructions by the manufacturer. Twenty-four hours after transfection, cells were fixed by 4% formaldehyde in PBS and DAPI stained before imaging on a confocal laser scanning microscope (SP5-AOBS; Leica Microsystems, Heidelberg, Germany) using a × 63 lens.

Immunoelectron microscopy

Immunoelectron microscopy was performed as previously described (van Weering *et al*, 2012). Briefly, HeLa cells expressing GFP–SNX1 were fixed in 4% PFA and 0.05% GA in phosphate buffer and processed according to the Tokuyasu method. In all, 70 nm sections were labelled with polyclonal rabbit anti-GFP (Molecular Probes, Invitrogen, Carlsbad, CA, USA) and Protein A-Gold (CMC, Utrecht, The Netherlands). The sections were counterstained with uranylacetate and analysed on a FEI Tecnai 12 Biotwin transmission electron microscope (FEI Company, Eindhoven, The Netherlands) at × 30 000 magnification.

Crystallography and structure determination

Residues 301–522 of human SNX1 (Swiss-Prot Q13596) were inserted into a modified pHIS2 vector encoding N-terminal 6 × His and MBP tags followed by a TEV cleavage site. His-MBP-SNX1 (301–522) was expressed in *Escherichia coli* BL21(DE3) cells (Novagen) in ZYM-5052 autoinduction medium (Studier, 2005). Cells were harvested by centrifugation after overnight growth at 20°C and stored at −80°C.

Frozen cells were resuspended in buffer A (50 mM Tris pH 7.7, 200 mM NaCl, 10 mM imidazole, 1 mM tris-(2-carboxyethyl)-phosphine (TCEP)), lysed in an Emulsiflex homogenizer (15 000 psi, Avestin, Canada) and centrifuged (40 min, 43 000 *g*). The supernatant was loaded onto an Ni^{2+}-IMAC column (HiTrap Chelating; GE Healthcare) and eluted with a 10–500 mM imidazole gradient. The 6 × His-MBP tag was subsequently removed by incubation with 20 μg/ml TEV protease at 4°C overnight. Following cleavage, the protein was diluted 10-fold with deionized water and loaded onto an anion exchange column (HiTrap Q; GE Healthcare) equilibrated with buffer B (20 mM Tris pH 7.8, 10 mM NaCl, 1 mM EDTA, 0.5 mM TCEP), and eluted with a 10–1000 mM NaCl gradient. Fractions containing SNX1 (301–522) were pooled, concentrated and loaded onto a gel filtration column (Sephadex 75; GE Healthcare) equilibrated with buffer C (20 mM Tris pH 7.8, 250 mM NaCl, 1 mM EDTA, 0.5 mM TCEP). Following gel filtration, SNX1 (301–522) was concentrated to 10–12 mg/ml and flash frozen in liquid N_2.

Crystals of SNX1 (301-522) were obtained by hanging drop vapour diffusion with drops that contained a 1:1 mixture of protein (10 mg/ml) and reservoir buffer D (1–3% PEG 20K, 0.1 M Tris pH 8.1). Rhombic crystals grew within a week and were cryoprotected by transfer into buffer D containing 30% PEG 400, followed by flash freezing in liquid N_2. A mercury derivative was obtained by overnight incubation of native crystals in buffer D containing 25% PEG 400 and 10 mM ethyl mercury phosphate (EMP).

A two-wavelength multiple anomalous diffraction (MAD) data set was collected at 100 K at beamline 22-BM at the Advanced Photon Source (Argonne, IL, USA) from an EMP derivative crystal. Native data were collected at a rotating anode home source (Table I). All data were processed with XDS and XSCALE. Mercury positions in the derivative data set were located with SHELXD and used for MAD phasing with SHARP. After solvent flattening as implemented in SHARP, the electron density clearly showed the positions of the alpha helices, allowing for initial tracing of helical elements at 3.4 Å using the ARP_helices module of ARP/wARP (Perrakis *et al*, 2001). The initial model was then placed into the unit cell of the native crystal and refined as a rigid body in REFMAC (Murshudov *et al*, 1997). Subsequent rounds of refinement with autoBUSTER (Blanc *et al*, 2004) and rebuilding with COOT (Emsley and Cowtan, 2004) resulted in a model with good stereochemistry and no residues in disallowed regions of the Ramachandran plot using RAMPAGE (Lovell *et al*, 2003; Table II). The SNX1 homodimer structure has been deposited in the RCSB with PDB code 4FZS.

Modelling

A multiple sequence alignment of the SNXs was performed using ClustalW2 (http://www.clustal.org/; Supplementary Figure S3B). The SNX1-SNX5 alignment was extracted and refined (Supplementary Figure S3C) to build the SNX5 homology model based on the SNX1 crystal structure reported in this study. Residue replacement, loop building and sidechain repacking were performed using InsightII (2005 version; Accelrys, San Diego, USA). Hydrogen atoms were added consistent with pH 7 and water added to a depth of 1 nm around the surface. The initial models were relaxed by energy minimization using the CVFF force-field in Discover (2.98 version; Accelrys) for a total of 4000 conjugate gradient steps. The protein backbone atoms were tethered to their initial positions at the start of the minimization and this restraint was gradually reduced to zero during the first 1000 steps. The stereo chemical quality of the models was assessed using PROCHECK (http://www.ebi.ac.uk/thornton-srv/software/PROCHECK/). Using the HHpred server (http://toolkit.tuebingen.mpg.de/hhpred) to search for both the best templates and best alignments for SNX8, which resulted in an alignment with the SNX9 structure. Based on this alignment, we constructed a homology model of SNX8 as described above.

Supplementary data

Supplementary data are available at *The EMBO Journal* Online (http://www.embojournal.org).

Acknowledgements

We would like to thank Mistuaki Tabuchi, Matthew Seaman, Mark Field, Martin Harterink and Koen van Grinsven for plasmids and cDNA. We thank Gamze Camdere and Harvey McMahon for advice on the liposome assays. Computational power for the molecular modelling was provided by Advanced Computing Research Centre, University of Bristol. Electron microscopy was performed at the Wolfson BioImaging Facility, University of Bristol. JRTvW is supported by the Wellcome Trust (085743). VKB and DS acknowledge financial support from the Lundbeck Foundation, and the University of Copenhagen programs of excellence 'BioScaRT' and 'UNIK-Synthetic Biology'. JHH is supported by the Intramural Program of the NIH, NIDDK. PJC is supported by the Wellcome Trust (089928/Z/09/Z and 085743) and the Royal Society.

Author contributions: JRTvW, JHH and PJC designed the project; JRTvW, RBS, CJT, DPK, SRC and PJC performed the experiments and contributed reagents; VKB and DS performed the bioinformatics; JRTvW, RBS, JHH and PJC wrote the manuscript.

Conflict of interest

The authors declare that they have no conflict of interest.

References

Bhatia VK, Madsen KL, Bolinger PY, Kunding A, Hedegård P, Gether U, Stamou D (2009) Amphipathic motifs in BAR domains are essential for membrane curvature sensing. *EMBO J* **28:** 3303–3314

Blanc E, Roversi P, Vonrhein C, Flensburg C, Lea SM, Bricogne G (2004) Refinement of severely incomplete structures with maximum likelihood in BUSTER-TNT. *Acta Crystallogr D Biol Crystallogr* **60:** 2210–2221

Boucrot E, Pick A, Çamdere G, Liska N, Evergren E, McMahon HT, Kozlov MM (2012) Membrane fission is promoted by insertion of amphipathic helices and is restricted by crescent BAR domains. *Cell* **149:** 124–136

Bujny MV, Popoff V, Johannes L, Cullen PJ (2007) The retromer component sorting nexin-1 is required for efficient retrograde transport of Shiga toxin from early endosome to the trans Golgi network. *J Cell Sci* **120:** 2010–2021

Carlton J, Bujny M, Peter B, Oorschot V, Rutherford A, Mellor H, Klumperman J, McMahon HT, Cullen PJ (2004) Sorting nexin-1 mediates tubular endosome-to-TGN transport through coincidence sensing of high- curvature membranes and 3-phosphoinositides. *Curr Biol* **14:** 1791–1800

Carlton J, Cullen PJ (2005) Sorting nexins. *Curr Biol* **15:** R819–R820

Cozier G, Carlton J, McGregor A, Gleeson P, Teasdale RD, Mellor H, Cullen PJ (2002) The phox homology (PX) domain-dependent, 3-phosphoinositide-mediated association of sorting nexin-1 with an early sorting endosomal compartment is required for its ability to regulate epidermal growth factor receptor degradation. *J Biol Chem* **277:** 48730–48736

Cullen PJ (2008) Endosomal sorting and signalling: an emerging role for sorting nexins. *Nat Rev Mol Cell Biol* **9:** 574–582

Cullen PJ, Korswagen HC (2012) Sorting nexins provide diversity for retromer-dependent trafficking events. *Nat Cell Biol* **14:** 29–37

Dislich B, Than ME, Lichtenthaler SF (2010) Specific amino acids in the BAR domain allow homodimerization and prevent heterodimerization of sorting nexin 33. *Biochem J* **433:** 75–83

Dyve AB, Bergan J, Utskarpen A, Sandvig K (2009) Sorting nexin 8 regulates endosome-to-Golgi transport. *Biochem Biophys Res Commun* **390:** 109–114

Emsley P, Cowtan K (2004) Coot: model-building tools for molecular graphics. *Acta Crystallogr D Biol Crystallogr* **60:** 2126–2132

Frost A, Perera R, Roux A, Spasov K, Destaing O, Egelman E, De Camilli P, Unger V (2008) Structural basis of membrane invagination by F-BAR domains. *Cell* **132:** 807–817

Gallop J, Jao C, Kent H, Butler P, Evans P, Langen R, McMahon HT (2006) Mechanism of endophilin N-BAR domain-mediated membrane curvature. *EMBO J* **25:** 2898–2910

Gautier R, Douguet D, Antonny B, Drin G (2008) HELIQUEST: a web server to screen sequences with specific alpha-helical properties. *Bioinformatics* **24:** 2101–2102

Geuze HJ, Slot JW, Strous GJ, Lodish HF, Schwartz AL (1983) Intracellular site of asialoglycoprotein receptor-ligand uncoupling: double-label immunoelectron microscopy during receptor-mediated endocytosis. *Cell* **32:** 277–287

Haberg K, Lundmark R, Carlsson S (2008) SNX18 is an SNX9 paralog that acts as a membrane tubulator in AP-1-positive endosomal trafficking. *J Cell Sci* **121:** 1495–1505

Habermann B (2004) The BAR-domain family of proteins: a case of bending and binding? *EMBO Rep* **5:** 250–255

Hettema EH, Lewis MJ, Black MW, Pelham HR (2003) Retromer and the sorting nexins Snx4/41/42 mediate distinct retrieval pathways from yeast endosomes. *EMBO J* **22:** 548–557

Hierro A, Rojas A, Rojas R, Murthy VN, Effantin G, Kajava A, Steven A, Bonifacino J, Hurley J (2007) Functional architecture of the retromer cargo-recognition complex. *Nature* **449:** 1063–1067

Huotari J, Helenius A (2011) Endosome maturation. *EMBO J* **30:** 3481–3500

Koumandou VL, Klute MJ, Herman EK, Nunez-Miguel R, Dacks JB, Field MC (2011) Evolutionary reconstruction of the retromer complex and its function in Trypanosoma brucei. *J Cell Sci* **124:** 1496–1509

Lovell SC, Davis IW, Arendall WB, de Bakker PI, Word JM, Prisant MG, Richardson JS, Richardson DC (2003) Structure validation by Calpha geometry: phi,psi and Cbeta deviation. *Proteins* **50:** 437–450

Mari M, Bujny M, Zeuschner D, Geerts W, Griffith J, Petersen C, Cullen PJ, Klumperman J, Geuze H (2008) SNX1 defines an early endosomal recycling exit for sortilin and mannose 6-phosphate receptors. *Traffic* **9:** 380–393

Mim C, Cui H, Gawronski-Salerno JA, Frost A, Lyman E, Voth GA, Unger VM (2012) Structural basis of membrane bending by the N-BAR protein endophilin. *Cell* **149:** 137–145

Murshudov GN, Vagin AA, Dodson EJ (1997) Refinement of macromolecular structures by the maximum-likelihood method. *Acta Crystallogr D Biol Crystallogr* **53:** 240–255

Norwood SJ, Shaw DJ, Cowieson NP, Owen DJ, Teasdale RD, Collins BM (2010) Assembly and solution structure of the core retromer protein complex. *Traffic* **12:** 56–71

Park J, Kim Y, Lee S, Park JJ, Park ZY, Sun W, Kim H, Chang S (2010) SNX18 shares a redundant role with SNX9 and modulates endocytic trafficking at the plasma membrane. *J Cell Sci* **123:** 1742–1750

Perrakis A, Harkiolaki M, Wilson KS, Lamzin VS (2001) ARP/wARP and molecular replacement. *Acta Crystallogr D Biol Crystallogr* **57:** 1445–1450

Peter BJ, Kent HM, Mills IG, Vallis Y, Butler PJ, Evans PR, McMahon HT (2004) BAR domains as sensors of membrane curvature: the amphiphysin BAR structure. *Science* **303:** 495–499

Pylypenko O, Lundmark R, Rasmuson E, Carlsson S, Rak A (2007) The PX-BAR membrane-remodeling unit of sorting nexin 9. *EMBO J* **26:** 4788–4800

Qualmann B, Koch D, Kessels MM (2011) Let's go bananas: revisiting the endocytic BAR code. *EMBO J* **30:** 3501–3515

Rutherford A, Traer C, Wassmer T, Pattni K, Bujny M, Carlton J, Stenmark H, Cullen PJ (2006) The mammalian phosphatidylinositol 3-phosphate 5-kinase (PIKfyve) regulates endosome-to-TGN retrograde transport. *J Cell Sci* **119:** 3944–3957

Seaman MN, McCaffery JM, Emr SD (1998) A membrane coat complex essential for endosome-to-Golgi retrograde transport in yeast. *J Cell Biol* **142:** 665–681

Seet L, Hong W (2006) The Phox (PX) domain proteins and membrane traffic. *Biochim Biophys Acta* **1761:** 878–896

Studier FW (2005) Protein production by auto-induction in high density shaking cultures. *Protein Expr Purif* **41:** 207–234

Teasdale RD, Collins BM (2012) Insights into the PX (phox-homology) domain and SNX (sorting nexin) protein families: structures, functions and roles in disease. *Biochem J* **441:** 39–59

Traer C, Rutherford A, Palmer K, Wassmer T, Oakley J, Attar N, Carlton J, Kremerskothen J, Stephens D, Cullen PJ (2007) SNX4 coordinates endosomal sorting of TfnR with dynein-mediated transport into the endocytic recycling compartment. *Nat Cell Biol* **9:** 1370–1380

van Weering JRT, Verkade P, Cullen PJ (2010) SNX-BAR proteins in phosphoinositide-mediated, tubular-based endosomal sorting. *Semin Cell Dev Biol* **21:** 371–380

van Weering JRT, Verkade P, Cullen PJ (2012) SNX-BAR-mediated endosome tubulation is co-ordinated with endosome maturation. *Traffic* **13:** 94–107

Wall DA, Wilson G, Hubbard AL (1980) The galactose-specific recognition system of mammalian liver: the route of ligand internalization in rat hepatocytes. *Cell* **21:** 79–93

Wang Q, Kaan HY, Hooda RN, Goh SL, Sondermann H (2008) Structure and plasticity of endophilin and sorting nexin 9. *Structure* **16:** 1574–1587

Wang Q, Navarro MV, Peng G, Molinelli E, Lin Goh S, Judson BL, Rajashankar KR, Sondermann H (2009) Molecular mechanism of membrane constriction and tubulation mediated by the F-BAR protein Pacsin/Syndapin. *Proc Natl Acad Sci USA* **106:** 12700–12705

Wassmer T, Attar N, Bujny M, Oakley J, Traer C, Cullen PJ (2007) A loss-of-function screen reveals SNX5 and SNX6 as potential components of the mammalian retromer. *J Cell Sci* **120:** 45–54

Wassmer T, Attar N, Harterink M, van Weering JRT, Traer CJ, Oakley J, Goud B, Stephens DJ, Verkade P, Korswagen HC, Cullen PJ (2009) The retromer coat complex coordinates endosomal sorting and dynein-mediated transport, with carrier recognition by the trans-Golgi network. *Dev Cell* **17:** 110–122

Zhang J, Zhang X, Guo Y, Xu L, Pei D (2009) Sorting nexin 33 induces Mammalian cell micronucleated phenotype and actin polymerization by interacting with wiskott-Aldrich syndrome protein. *J Biol Chem* **284:** 21659–21669

